

Finite temperature effects on the structural stability of Si-doped HfO₂ using first-principles calculations

Y. Harashima,^{1,2,*} H. Koga,³ Z. Ni,⁴ T. Yonehara,³ M. Katouda,³ A. Notake,⁵
H. Matsui,⁴ T. Moriya,⁵ M. K. Si,² R. Hasunuma,⁶ A. Uedono,⁶ and Y. Shigeta²

¹*Division of Materials Science, Nara Institute of Science and Technology, Ikoma 630-0192, Japan*

²*Center for Computational Sciences, University of Tsukuba, Tsukuba 305-8577, Japan*

³*Department of Computational Science and Technology,*

Research Organization for Information Science and Technology, Tokyo 105-0013, Japan

⁴*S-Technology Development Center, Tokyo Electron Technology Solutions Ltd.*

⁵*Advanced Data Planning Department, Tokyo Electron Ltd.*

⁶*Faculty of Pure and Applied Science, University of Tsukuba, Tsukuba 305-8573, Japan*

(Dated: March 28, 2023)

The structural stabilities of the monoclinic and tetragonal phases of Si-doped HfO₂ at finite temperatures were analyzed using a computational scheme to assess the effects of impurity doping. The finite temperature effects considered in this work represented lattice vibration and impurity configuration effects. The results show that 6% Si doping stabilizes the tetragonal phase at room temperature, although a higher concentration of Si is required to stabilize the tetragonal phase at zero temperature. These data indicate that lattice vibration and impurity configuration effects are important factors determining structural stability at finite temperatures.

INTRODUCTION

Hafnium-based materials, typically HfO₂, have found numerous applications in the semiconductor industry as high-k dielectric compounds [1] and are also promising ferroelectric and antiferroelectric materials [2]. These compounds were first employed in the 200s, such as during the 45 nm technology node in 2007 [3] and in certain earlier applications in dynamic random-access memory [4]. The application of high-k materials allowed the continued scaling of various devices by suppressing the gate leakage associated with greater physical thicknesses exhibited by conventional SiO₂ dielectric materials. Since then, HfO₂ and analogues obtained by doping have become crucial components of many advanced device structures, ranging from gate-all-around transistors [5] to post-silicon 2D channels such as transition metal dichalcogenides [6, 7].

The exceptional electronic properties of HfO₂ appear primarily in the tetragonal and orthorhombic phases. Notably, the dielectric constant, κ , of tetragonal HfO₂ is ~ 30 and so is approximately twice that of stable monoclinic HfO₂ [8]. However, the tetragonal and orthorhombic phases are not stable at room temperature [8, 9]. Consequently, to allow the application of these materials in various devices, it is important to develop techniques to stabilize the tetragonal phase.

Techniques for controlling the phase have been developed through doping of impurities at different concentration. As an example, a prior study produced a Si-doped HfO₂ thin film having a ferroelectric orthogon structure [10, 11]. Additionally, recent experimental work fabricated heterogeneous Hf_{1-x}Zr_xO₂ almost entirely composed of a non-monoclinic phase using physical vapor deposition with a composition depth profile suggested by a machine learning model (that is, using Bayesian optimization) [12]. Fischer *et al.* studied doping with the group IV elements Si, C, Ge, Sn, Ti and Ce into bulk HfO₂ [13, 14] and found that Si and Ge stabi-

lize the tetragonal structure. Doping with Si, P, Ge, Al, Y, Ti, Zr, Gd and Sc was also investigated in HfO₂ by Lee *et al.* [15], who identified the microscopic mechanisms by which these dopants stabilize the tetragonal structure on the basis of ionic radii. In other work [16], possible metastable phases of HfO₂ were analyzed using first-principles calculations. As well, a systematic screening of dopants capable of inducing ferroelectric characteristics in HfO₂ has been performed [17].

When assessing the viability of synthesizing a particular phase, a theoretical analysis of the structural stability at finite temperatures is required. In addition, the total energies obtained from first-principles calculations based on density functional theory indicate structural stability at zero temperature. To investigate the stabilization imparted by doping with impurities at finite temperatures, it is necessary to consider both lattice vibration effects and impurity configuration effects. In a previous study [14], calculations were performed that incorporated the lattice vibrational free energy based on considering phonon dispersion. Typically, the impurity configuration is assumed to be homogeneous, such that the impurity atoms are periodically aligned within the host lattice. Recently the authors performed a systematic search for elements capable of stabilizing HfO₂ and ZrO₂ using first-principles calculations [18]. In this prior work, several impurity atoms were included in a supercell and the total energies for all possible impurity configurations in the supercell were estimated. In this manner, the most stable configuration at zero temperature was ascertained. The results indicated that Si substituted at 6 % was aligned along linearly and thus not homogeneously distributed throughout the host matrix, suggesting that the dopant configuration cannot be neglected when calculating energy values.

The present study investigated the finite temperature phase stability of Si-doped HfO₂, based on a computational scheme that simultaneously considered lattice vibration and impurity configuration effects. On the basis of the results, the transfor-

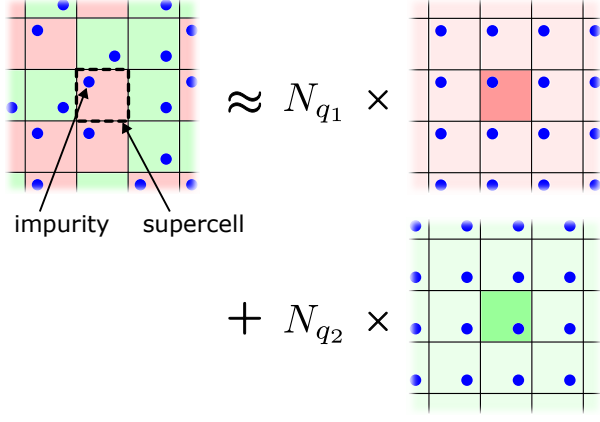


FIG. 1. Schematic of the model used to approximate impurity configurations, showing a configuration Λ is shown. The left-hand side of the figure presents two types of supercells, q_1 (red) and q_2 (green), having different impurity configurations. The impurities are indicated by blue spheres. The overall system is modeled as a combination of supercells and the contribution from each cell is approximated by that of a piece of a system in which the pieces are aligned periodically. Two periodically aligned systems (q_1 -type and q_2 -type) are considered, as shown in the right-hand side of the figure, and the electronic states and vibrational modes for these two systems are calculated. Here, N_{q_1} and N_{q_2} are the numbers of the two types of cells in the entire system.

mation between the tetragonal and monoclinic phases of HfO_2 in association with Si doping is discussed. The data indicate that 6% Si doping stabilizes the tetragonal structure at room temperature while the monoclinic structure is the most stable at zero temperature.

METHODS

This work determined the free energies of impurity substituted systems considering impurity configurations and lattice vibrations. The calculations are based on a system having impurity configuration Λ and lattice vibrational degrees of freedom Γ . The state of Γ is dependent on Λ but this relationship is not explicitly written. In this process, the partition function Z is expressed as the sum over all possible of Λ , written as

$$Z = \sum_{\Lambda} \sum_{\Gamma} \exp(-\beta E_{\Lambda}(\Gamma)) \quad (1)$$

$$= \sum_{\Lambda} Z_{\Lambda}, \quad (2)$$

$$Z_{\Lambda} \equiv \sum_{\Gamma} \exp(-\beta E_{\Lambda}(\Gamma)). \quad (3)$$

Here, $E_{\Lambda}(\Gamma)$ denotes the electronic and vibrational energy of the configuration Λ and Z_{Λ} is the partition function for this configuration. It is not feasible to calculate the exact value of Z or even of Z_{Λ} because the system size is very large (or even

infinite at the thermodynamic limit). Therefore, the system is separated into supercells and the energy of the overall system is approximated by summing over these supercells. This process can be expressed in terms of Z_{Λ} as

$$Z_{\Lambda} = \prod_I z_I. \quad (4)$$

In this case, the impurities are distributed in each supercell I . The energies for a single supercell I can be approximated as the energies for a system of periodically aligned impurities (see Fig. 1). Considering the free energy f_I of a periodically aligned supercell, we can write

$$Z_{\Lambda} \approx \prod_I \sum_{\gamma_I} \exp(-\beta e_I(\gamma_I)) \quad (5)$$

$$= \prod_I \exp(-\beta f_I) \quad (6)$$

$$= \exp\left(-\beta \sum_I f_I\right). \quad (7)$$

Here, e_I denotes the energy of supercell I . These energies include contributions from vibrational modes γ_I in the approximated periodic system, such that the free energy f_I in cell I is

$$f_I \equiv -\frac{1}{\beta} \ln \sum_{\gamma_I} \exp(-\beta e_I(\gamma_I)). \quad (8)$$

Note that this f_I is the value per supercell. Because the supercell size is finite, there is only a finite number of impurity configuration patterns that need to be considered. The partition function for the overall system is therefore written in terms of the free energy f_q of each pattern q as

$$Z \approx \sum_{\Lambda} \exp\left(-\beta \sum_I f_I\right) \quad (9)$$

$$= \sum_{\Lambda} \exp\left(-\beta N \sum_q n_q f_q\right) \quad (10)$$

$$= \sum_{\{n_q\}} W_{\{n_q\}} \exp\left(-\beta N \sum_q n_q f_q\right), \quad (11)$$

where n_q is the proportion of cells having pattern q in the entire system and N is the number of supercells which, as noted, will be huge or even infinite at the thermodynamic limit. The energy value is approximated by summing over the patterns and the summation over Λ can be obtained by summation over $\{n_q\}$, as when going from Eq. (10) to (11). Using Stirling's approximation, the weight $W_{\{n_q\}}$ can be estimated as

$$W_{\{n_q\}} = \frac{N!}{\prod_q N_q!} \approx \exp\left(-N \sum_q n_q \ln n_q\right). \quad (12)$$

N_q denotes $N n_q$. Substituting Eq. (12) to Eq. (11), we obtain

$$Z \approx \sum_{\{n_q\}} \exp\left(-\beta N \sum_q n_q \left(f_q + \frac{1}{\beta} \ln n_q\right)\right). \quad (13)$$

At the thermodynamic limit ($N \rightarrow \infty$), the most probable set $\{n_q\}$ is realized and this set satisfies the conditions

$$\frac{\partial}{\partial n_q} \sum_q n_q \left(f_q + \frac{1}{\beta} \ln n_q \right) = 0, \quad (14)$$

$$\sum_q n_q = 1. \quad (15)$$

By solving this equation, we obtain

$$n_q = \frac{\exp(-\beta f_q)}{\sum_{q'} \exp(-\beta f_{q'})}. \quad (16)$$

The dominant contribution in Eq. (13) is given by the set of Eq. (16). Taking the logarithm, the free energy per supercell can be written as

$$f \equiv \frac{F}{N} = -\frac{1}{\beta N} \ln Z \approx -\frac{1}{\beta} \ln \left[\sum_q \exp(-\beta f_q) \right]. \quad (17)$$

This formula includes the contributions of configurational entropy, by summing over q , and of vibrational free energy via f_q . The derivation of this formula is similar to that of the canonical ensemble but uses f_q , instead of energy.

RESULTS AND DISCUSSION

The relationships derived in the preceding section were employed to analyze the phase stability of Si-doped HfO₂. HfO₂ can exist as a monoclinic phase having a low dielectric constant or a tetragonal phase having a high dielectric constant. The former is stable at room temperature and the transformation from the monoclinic to the tetragonal phases occurs at 2052 K [19]. Here, the free energy values for both phases at finite temperatures were compared.

The f_q term was obtained using first-principles calculations, employing the Vienna Ab initio Simulation Package (VASP) based on the projector augmented-wave method [20–22]. The generalized gradient approximation was also employed for the exchange-correlation energy functional [23]. The crystal structures were numerically optimized based on preserving the lattice symmetry of the pristine compound and applying $a = b$ and $\alpha = \beta = \gamma = \pi/2$ for the tetragonal phase and $a = b$ and $\alpha = \gamma = \pi/2$ for the monoclinic phase. Each dimension of the supercell was twice that of the conventional cell ($2 \times 2 \times 2$ of the conventional cell), which contains 96 atoms in total. The impurity configuration patterns could be classified into several groups based on spatial symmetry. As an example, 2 Hf substitutions in the tetragonal $2 \times 2 \times 2$ supercell can produce ${}_{32}C_2 = 496$ impurity configurations that can be classified into nine symmetrically equivalent groups. The supercell code [24] was used to identify these groups. The 496 configurations are separated into 128 patterns \times 2 groups, 64 patterns \times 2 groups, 32 patterns \times 2 groups, and 16 patterns \times 3 groups. 2 Hf substitution into the monoclinic supercell produces 23 groups which contains 32×8 and 16×15

groups. In the case of practical calculations (that is, for 2 Hf substitutions in the tetragonal structure), Eq. (17) is estimated as

$$f = -\frac{1}{\beta} \ln \left[\sum_{q'=1}^9 M_{q'} \cdot \exp(-\beta f_{q'}) \right], \quad (18)$$

$$M_{q'} = \{128, 128, 64, \dots\}, \quad (19)$$

such that nine $f_{q'}$ values can be calculated using first-principles calculations as explained below. By comparing f for the tetragonal and monoclinic phases, the effect of temperature on phase stability and the structural transformation temperature could be obtained.

In this study, the vibrational free energy of each impurity configuration, f_q , was estimated using the Debye-Grüneisen model [25] based on the equations

$$F_{q'}(V, T) = E_{\text{el}}(V) - k_{\text{B}}T \left[D\left(\frac{\Theta_{\text{D}}}{T}\right) - 3 \ln \left(1 - \exp\left(-\frac{\Theta_{\text{D}}}{T}\right) \right) \right] + \frac{9}{8} k_{\text{B}} \Theta_{\text{D}}, \quad (20)$$

$$\Theta_{\text{D}} = (6\pi^2)^{\frac{1}{3}} \frac{\hbar}{k_{\text{B}}} v^{\frac{1}{6}} \left(\frac{B}{m}\right)^{\frac{1}{2}}, \quad (21)$$

and

$$D(x) = \frac{3}{x^3} \int_0^x dx' \frac{x'^3}{e^{x'} - 1}, \quad (22)$$

where Θ_{D} and $D(x)$ are the Debye temperature and Debye function, respectively. v and m are averaged volume and mass per atom in supercell, and B is a bulk modulus. The free energy term $F_{q'}$ in Eq. (20) is calculated by first ascertaining the bulk modulus. This can be accomplished by considering the Murnaghan equation of states

$$B(p) = B_0 + B'_0 p = B_0 \left(\frac{V}{V_0}\right)^{-B'_0}, \quad (23)$$

$$E_{\text{el}}(V) = E_0 - \frac{B_0}{B'_0} V_0 \left[\frac{1}{1 - B'_0} \left(\frac{V}{V_0}\right)^{1 - B'_0} - \frac{V}{V_0} - \frac{B'_0}{1 - B'_0} \right]. \quad (24)$$

The total energies were calculated for volumes expanded and contracted from the stable structure by several percent and B_0 and B'_0 were obtained by regression of these total energies. The stable lattice structure for a given temperature was determined as the minimum value of Eq. (20) and the free energy values were estimated for an arbitrary temperature. It should be noted that the present approach involved a systematic error. Specifically, the structural transformation temperatures for pristine HfO₂ and ZrO₂ were estimated using this process as benchmarks and values of 1000 K and 750 K were obtained. These values are scaled by a factor of 2 with respect to the experimental data, and so the calculated transformation temperatures for the doped systems should possible be scaled

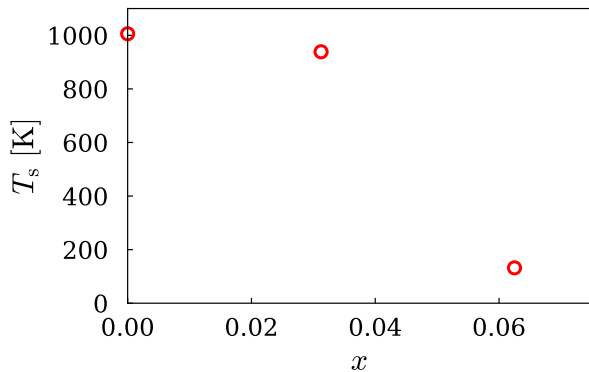


FIG. 2. The transformation temperature as a function of the extent of Si doping in $\text{Hf}_{1-x}\text{Si}_x\text{O}_2$.

by a factor of 2 as well. The accuracy of these calculations could possibly be improved by replacing the process used to assess vibrational modes with first-principles phonon calculations [26–29]. More sophisticated calculations such as these will be examined in future work.

The transformation temperature was estimated based on the crossing point of the free energies of the tetragonal and monoclinic phases. Figure 2 plots the structural transformation temperature T_s of HfO_2 versus the extent of Si doping and demonstrates that the correlation between the two is not linear. The T_s value for 3% Si doping is almost the same as that of the pristine compound but rapidly decreases as the extent of substitution increases from 3% to 6%. The decreasing trend against Si concentration is consistent with the results of the previous studies. [14] The T_s value determined for 6% substitution was 130 K. Although, as noted, this temperature may be underestimated and could possibly be scaled by a factor of 2, the value would still be lower than room temperature. This finding indicates that a 6% Si-doped HfO_2 dielectric layer in a typical device will exist in the tetragonal phase at a normal operating temperature.

The temperature dependence of the impurity configurations was also examined. The proportion of each impurity configuration in a system defined as in Eq. (16) can be estimated from the f_q calculated for each temperature. In the tetragonal phase, a single configuration (and symmetrically equivalent configurations) was dominant up to $\simeq 1500$ K. In contrast, in the case of the monoclinic phase, three impurity configurations appeared depending on temperature. Figure 3 summarizes the effect of temperature on n_q for the monoclinic phase. It is evident that the most stable configuration varied with temperature, indicating that the local structure of the impurities affected phase stability. Even though the calculated transformation temperature was lower than the temperatures at which several configurations were mixed, $\simeq 250$ K or $\simeq 800$ K, the temperatures at which such compounds are synthesized will be similar to or much higher than these values. Hence, it is

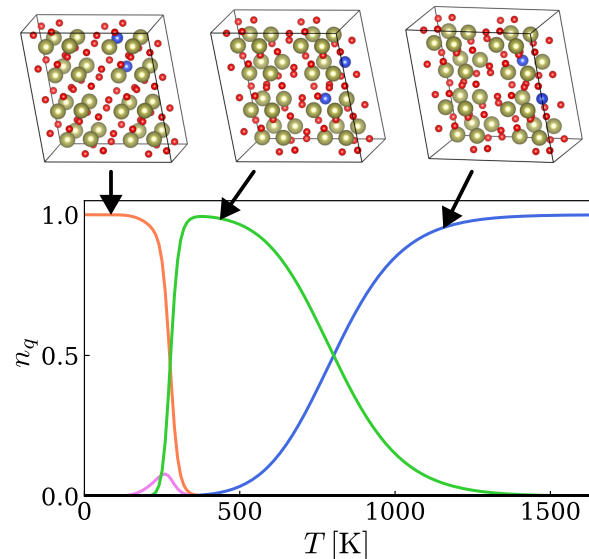


FIG. 3. Effect of temperature on the proportion n_q of the monoclinic phase (including the multiplicity M_q). The most probable configurations are shown in the upper panels at the various temperatures. The gold, red and blue spheres denote Hf, O and Si, respectively.

important to take into account the appearance of several configurations during the synthetic process.

CONCLUSION

This work analyzed the structural stability of Si-doped HfO_2 using the scheme that estimated the free energy and considered impurity configurations and lattice vibrations. The present process is evidently a useful means of assessing the phase stability of doped polymorphic compounds. The structural transformation from the monoclinic phase to the tetragonal phase was also investigated based on analyzing the free energy difference. The transformation temperature values indicate that a tetragonal structure with 6% Si doping will be stable at room temperature while a monoclinic structure is more stable at zero temperature. In the case of a device operating at room temperature, doping with 6% Si was found to be sufficient to stabilize the tetragonal HfO_2 phase.

In general, the physical properties of a compound will be highly correlated with its crystal structure, as demonstrated by the HfO_2 used in this work as a model case. The proposed method in this paper is expected to be applicable to a variety of scenarios. As an example, in permanent magnets, certain compounds exhibit excellent magnetic properties but are unstable and so it is important to stabilize these substances [30–33]. In particular, stabilization at the high temperatures at which these compounds are synthesized has recently attracted much attention [34]. We expect that the method demonstrated

herein will be effective in such cases and could be helpful in the search for structural stabilizers.

This work was supported by JSPS KAKENHI grant number JP22K03449. The computation was partly conducted using the facilities of the Supercomputer Center at the Institute for Solid State Physics in the University of Tokyo, the Multi-disciplinary Cooperative Research Program at the Center for Computational Sciences in University of Tsukuba, Subsystem B of the ITO system in Kyushu University, and Research Center for Computational Science, Okazaki, Japan (Project: 22-IMS-C104).

* harashima.yosuke@ms.naist.jp

- [1] G. D. Wilk, R. M. Wallace, and J. M. Anthony, *Journal of Applied Physics* **89**, 5243 (2001), <https://doi.org/10.1063/1.1361065>.
- [2] M. H. Park, Y. H. Lee, H. J. Kim, Y. J. Kim, T. Moon, K. D. Kim, J. Müller, A. Kersch, U. Schroeder, T. Mikolajick, and C. S. Hwang, *Advanced Materials* **27**, 1811 (2015), <https://onlinelibrary.wiley.com/doi/pdf/10.1002/adma.201404531>.
- [3] K. Mistry, C. Allen, C. Auth, B. Beattie, D. Bergstrom, M. Bost, M. Brazier, M. Buehler, A. Cappellani, R. Chau, C.-H. Choi, G. Ding, K. Fischer, T. Ghani, R. Grover, W. Han, D. Hanken, M. Hattendorf, J. He, J. Hicks, R. Huessner, D. Ingerly, P. Jain, R. James, L. Jong, S. Joshi, C. Kenyon, K. Kuhn, K. Lee, H. Liu, J. Maiz, B. McIntyre, P. Moon, J. Neiryneck, S. Pae, C. Parker, D. Parsons, C. Prasad, L. Pipes, M. Prince, P. Ranade, T. Reynolds, J. Sandford, L. Shifren, J. Sebastian, J. Seiple, D. Simon, S. Sivakumar, P. Smith, C. Thomas, T. Troeger, P. Vandervoorn, S. Williams, and K. Zawadzki, in *2007 IEEE International Electron Devices Meeting* (2007) pp. 247–250.
- [4] S. K. Kim and M. Popovici, *MRS Bulletin* **43**, 334 (2018).
- [5] T. Ernst, C. Dupre, C. Isheden, E. Bernard, R. Ritzenthaler, V. Maffini-Alvaro, J.-C. Barbe, F. De Crecy, A. Toffoli, C. Vizioz, S. Borel, F. Andrieu, V. Delaye, D. Lafond, G. Rabille, J.-M. Hartmann, M. Rivoire, B. Guillaumot, A. Suhm, P. Rivallin, O. Faynot, G. Ghibaudo, and S. Deleonibus, in *2006 International Electron Devices Meeting* (2006) pp. 1–4.
- [6] W. Li, J. Zhou, S. Cai, Z. Yu, J. Zhang, N. Fang, T. Li, Y. Wu, T. Chen, X. Xie, K. Ma, Haibo Yan, N. Dai, X. Wu, H. Zhao, Z. Wang, D. He, L. Pan, Y. Shi, P. Wang, W. Chen, K. Nagashio, X. Duan, and X. Wang, *Nature Electronics* **2**, 563 (2019).
- [7] P. Xia, X. Feng, R. J. Ng, S. Wang, D. Chi, C. Li, Z. He, X. Liu, and K.-W. Ang, *Scientific Reports* **7**, 40669 (2017).
- [8] K. Tomida, K. Kita, and A. Toriumi, *Applied Physics Letters* **89**, 142902 (2006), <https://doi.org/10.1063/1.2355471>.
- [9] J. Wang, H. P. Li, and R. Stevens, *Journal of Materials Science* **27**, 5397 (1992).
- [10] T. S. Böske, J. Müller, D. Bräuhaus, U. Schröder, and U. Böttger, *Applied Physics Letters* **99**, 102903 (2011), <https://doi.org/10.1063/1.3634052>.
- [11] T. S. Böske, S. Teichert, D. Bräuhaus, J. Müller, U. Schröder, U. Böttger, and T. Mikolajick, *Applied Physics Letters* **99**, 112904 (2011), <https://doi.org/10.1063/1.3636434>.
- [12] Z. Ni and H. Matsui, *Japanese Journal of Applied Physics* **61**, SH1009 (2022).
- [13] D. Fischer and A. Kersch, *Applied Physics Letters* **92**, 012908 (2008), <https://aip.scitation.org/doi/pdf/10.1063/1.2828696>.
- [14] D. Fischer and A. Kersch, *Journal of Applied Physics* **104**, 084104 (2008), <https://doi.org/10.1063/1.2999352>.
- [15] C.-K. Lee, E. Cho, H.-S. Lee, C. S. Hwang, and S. Han, *Phys. Rev. B* **78**, 012102 (2008).
- [16] S. V. Barabash, *J. Comput. Electron.* **16**, 1227 (2017).
- [17] R. Batra, T. D. Huan, G. A. J. Rossetti, and R. Ramprasad, *Chemistry of Materials* **29**, 9102 (2017), <https://doi.org/10.1021/acs.chemmater.7b02835>.
- [18] Y. Harashima, H. Koga, Z. Ni, T. Yonehara, M. Katouda, A. Notoake, H. Matsui, T. Moriya, M. K. Si, R. Hasunuma, A. Uedono, and Y. Shigeta, in *2022 International Symposium on Semiconductor Manufacturing (ISSM)* (2022) pp. 1–3.
- [19] C. Wang, M. Zinkevich, and F. Aldinger, *Journal of the American Ceramic Society* **89**, 3751 (2006), <https://ceramics.onlinelibrary.wiley.com/doi/pdf/10.1111/j.1551-2916.2006.01286.x>.
- [20] P. E. Blöchl, *Phys. Rev. B* **50**, 17953 (1994).
- [21] G. Kresse and J. Furthmüller, *Phys. Rev. B* **54**, 11169 (1996).
- [22] G. Kresse and D. Joubert, *Phys. Rev. B* **59**, 1758 (1999).
- [23] J. P. Perdew, K. Burke, and M. Ernzerhof, *Phys. Rev. Lett.* **77**, 3865 (1996).
- [24] K. Okhotnikov, T. Charpentier, and S. Cadars, *J. Cheminform.* **8**, 17 (2016).
- [25] V. L. Moruzzi, J. F. Janak, and K. Schwarz, *Phys. Rev. B* **37**, 790 (1988).
- [26] A. Togo and I. Tanaka, *Scripta Materialia* **108**, 1 (2015).
- [27] T. Tadano, Y. Gohda, and S. Tsuneyuki, *Journal of Physics: Condensed Matter* **26**, 225402 (2014).
- [28] A. Kuwabara, T. Tohei, T. Yamamoto, and I. Tanaka, *Phys. Rev. B* **71**, 064301 (2005).
- [29] X. Luo, W. Zhou, S. V. Ushakov, A. Navrotsky, and A. A. Demkov, *Phys. Rev. B* **80**, 134119 (2009).
- [30] T. Miyake, K. Terakura, Y. Harashima, H. Kino, and S. Ishibashi, *J. Phys. Soc. Jpn.* **83**, 043702 (2014).
- [31] Y. Harashima, K. Terakura, H. Kino, S. Ishibashi, and T. Miyake, *J. Appl. Phys.* **120**, 203904 (2016).
- [32] Y. Harashima, T. Fukazawa, H. Kino, and T. Miyake, *J. Appl. Phys.* **124**, 163902 (2018).
- [33] Y. Harashima, T. Fukazawa, and T. Miyake, *Scripta Materialia* **179**, 12 (2020).
- [34] G. Xing, T. Ishikawa, Y. Miura, T. Miyake, and T. Tadano, *Journal of Alloys and Compounds* **874**, 159754 (2021).